Published in 2021:
Insight – Non-Destructive Testing and Condition Monitoring **63**(1): 28-36, Jan 2021.

Prediction of reflection amplitudes for ultrasonic inspection of rough planar defects

S.G. Haslinger[1,2], M.J.S. Lowe[2], R.V. Craster[2,3], P. Huthwaite[2] and F. Shi[4]

[1] Department of Mathematical Sciences, University of Liverpool

[2] Department of Mechanical Engineering and [3] Department of Mathematics, Imperial College London

[4] Department of Mechanical and Aerospace Engineering, Hong Kong University of Science and Technology

Abstract:

The characteristics of planar defects (no loss of material volume) that arise during industrial plant operation are difficult to predict in detail, yet these can affect the performance of NDT used to manage plant structural integrity. Inspection modelling is increasingly used to design and assess ultrasonic inspections of such plant items. While modelling of smooth planar defects is relatively mature and validated, issues have remained in the treatment of rough planar defect species. The qualification of ultrasonic inspections for such defects is presently very conservative, owing to the uncertainty of the amplitudes of rough surface reflections. Pragmatic solutions include the addition of large sensitivity thresholds and more frequent inspection intervals which require more plant down-time. In this article, an alternative approach has been developed by the authors to predict the expected surface reflection from a rough defect using a theoretical statistical model. Given only the frequency, angle of incidence and two statistical parameter values used to characterise the defects, the expected reflection amplitude is obtained rapidly for any scattering angle and size of defect, for both compression and shear waves. The method is applicable for inspections of isotropic media that feature surface reflections such as Pulse-Echo or Pitch-Catch, rather than for tip signal dependent techniques such as time-of-flight diffraction. The potential impact for inspection qualification is significant with the new model predicting increases of up to 20dB in signal amplitude in comparison with models presently used in industry. All mode conversions are included and rigorous validations using numerical and experimental methods were performed. The model has been instrumental in obtaining new statistically significant results related to the effect of tilt; the expected pulse-echo backscattered amplitude for very rough planar defects is independent of tilt angle, with convergence obtained for a range of frequencies.

Section 1: Introduction and application to industry

The inspection of safety-critical components in the nuclear power industry uses procedures to detect defects to a specified threshold of severity. These thresholds are provided by inspection qualification documents, which include information related to defect length/through-wall extent (TWE), morphology, tilt & skew angles, sizing and location tolerances etc. [1]. Rough surfaces of defects affect the scattering of ultrasonic waves and significantly reduce the signal amplitude in the specular direction compared with that of a smooth defect [2]. Predictions for the expected amplitudes of reflected waves are required to qualify safety-critical inspections by setting amplitude thresholds.

Although this can be done reliably for smooth cracks, rough defects are more problematic due to their unique randomness, so the only recourse in current practice is to adopt very conservative assumptions for the expected reflection.

This article presents a statistical model capable of rapidly predicting the amplitude of waves reflected by rough surfaces, and with improvements of the safety margin by up to 20dB compared with established models [3]. Figure 1 shows an example in three-dimensional space (3D) for stainless steel with typical material parameters $E = 210\ \mathrm{GPa}, \rho = 7800\ \mathrm{kg/m^3}, \upsilon = 0.29\ (c_\mathrm{p} = 5940\ \mathrm{m/s}, c_\mathrm{s} = 3230\mathrm{m/s})$.

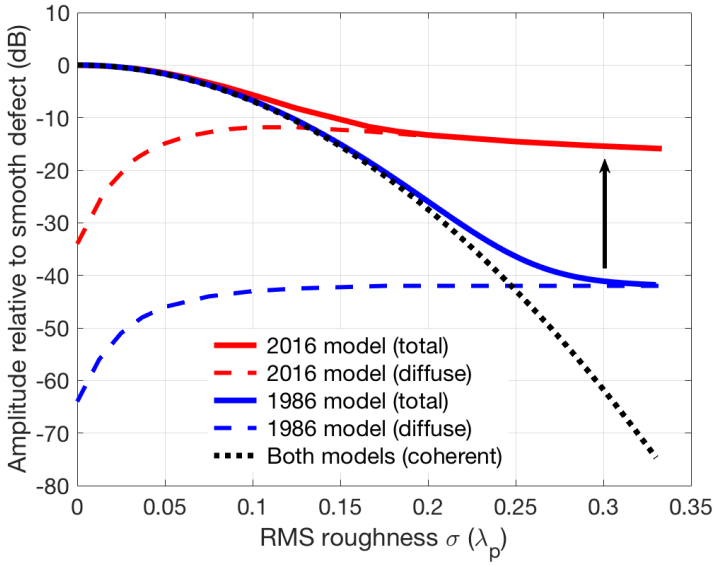

Figure 1: *Expected reflection amplitude (relative to a smooth defect of the same size, 10mm by 10mm) vs RMS roughness (measured in incident wavelengths) for normally incident compression waves in a 3D Pulse-Echo set-up with centre frequency 10MHz for a fixed value of correlation length (half the incident wavelength). The solid red line is the predicted P-P amplitude using the new model (2016, [4]), with the solid blue line the prediction using the 1986 model [3]. Dashed lines represent the diffuse parts from 1986 and 2016 and the dotted black line represents the coherent field used in both models.*

Figure 1 depicts the comparison of a model by Ogilvy from 1986 [3], and the new method presented here, to predict the expected reflected signal from a rough surface (10mm by 10mm) for normally incident compression waves with centre frequency 10MHz. The two models match well for roughness up to 1/10 of the incident wavelength. As roughness increases, the model predictions diverge, the reasons for which will be explained in what follows. Note that as roughness increases, the solid red curve in Figure 1 flattens (compared with the solid blue curve predicted by [3]), indicating that reliable predictions for expected reflection amplitudes may be made for very rough defects without knowledge of the precise statistical descriptors of the roughness.

A study for compression waves using finite element (FE) simulations [2] illustrated the over-conservatism of the predictions for the total scattered field provided by [3], for the case of normal incidence. A comparison of Figure 8 in [3] and Figure 14 in [2] shows that the expected amplitude of the industry-adopted model of [3] is overly conservative by at least 20dB once roughness surpasses a specific threshold. This result was the motivation for the new theoretical model summarized here that includes elastic waves and all mode conversions [4-8].

Well-established acoustic theories are known for rough surface scattering (see, for example, [9,10]) but neglect the phenomenon of mode conversion, which can account for considerable signal amplitude reduction. In early influential work, Ogilvy [11-12] used Kirchhoff approximation (KA) theory to provide formulae for expected amplitudes for elastic wave scattering. Subsequent numerical and theoretical investigations also implemented KA methods for modelling relevant elastodynamic scattering problems [2, 13-14]. An important part of the approach is that the total scattered field may be considered as a sum of two parts: the coherent contribution and the diffuse part.

The coherent field is in the specular direction and for surfaces of the same statistical class, is in constant phase [15]. The diffuse field characterizes the rough nature of the surface, being the random component of the ultrasonic signal spread over all scattering directions. A schematic illustration is shown in Figure 2 for a moderately rough surface. The dominant coherent part of the signal is in the specular direction but the non-trivial roughness contributes a diffuse scattered signal, spread over all directions.

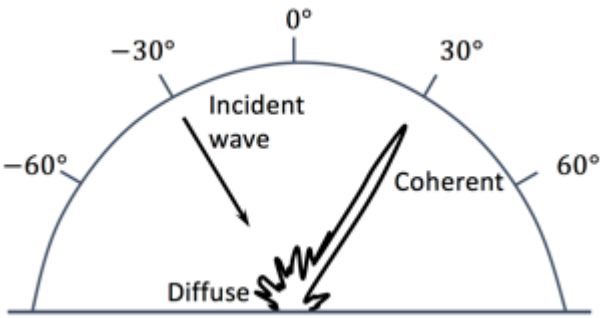

Figure 2: Schematic illustration of coherent and diffuse parts of a scattered field using a polar plot of scattered amplitudes for a plane wave incident on an infinite rough surface at $30°$.

The constant phase of coherent contributions means that Monte Carlo (MC) stochastic methods are effective for obtaining statistical predictions for rough surface scattering, since the total and coherent fields possess distinct definitions:

$$U^{\mathrm{t}} = \frac{1}{N}\sum_{n=1}^{N} |u_n^{\mathrm{sc}}(\theta_{\mathrm{sc}})| \;; \quad U^{\mathrm{c}} = \left|\frac{1}{N}\sum_{n=1}^{N} u_n^{\mathrm{sc}}(\theta_{\mathrm{sc}})\right|, \tag{1}$$

where *N* is the number of rough surfaces (or realisations) for a statistical class of roughness in an MC study, and the superscripts t, c, sc represent total, coherent and scattered, respectively. The terms U^{t} and U^{c} denote, respectively, the total and coherent **amplitudes** of the scattered field. The corresponding **intensities** are defined by:

$$I^{\mathrm{t}} = \frac{1}{N}\sum_{n=1}^{N} |u_n^{\mathrm{sc}}(\theta_{\mathrm{sc}})|^2 \;; \quad I^{\mathrm{c}} = \left|\frac{1}{N}\sum_{n=1}^{N} u_n^{\mathrm{sc}}(\theta_{\mathrm{sc}})\right|^2. \tag{2}$$

Note that the differences in the definitions of the ensemble averages in (1), (2) have a profound effect on the contribution of phase to the resulting calculations. As explained by Ogilvy [3,15], U^{c} contains no contribution from the diffuse, or incoherent, part of the scattered signal. In the specular direction, the signals have the same phase meaning their sum produces a large value. Away from the specular direction, the signals will be of random phase; their sum tends to zero (provided that the ensemble average is calculated over a sufficiently large number of surfaces), causing the diffuse

contribution to vanish if an ensemble average is performed in this way. To derive a realistic prediction for the total scattered field, a theoretical expression for the total intensity I^{t} (which includes phase consideration in the ensemble averaging technique) is required.

As will be explained in Section 2.2, an equation for the coherent amplitude/coherent intensity was obtained in the 1980s but the accompanying estimate for the diffuse field was approximated as a difference between the coherent field for a rough defect and the specular component for a smooth defect of the same size [3]. An underlying assumption was that in the far field, the diffuse field scatters equally in all directions, thereby removing angular dependence from the theoretical prediction. It was hypothesized that errors would occur for intermediate roughness, but that the results should work well in the limits of a smooth surface and an extremely rough surface [3]. Our new model shows that even for very rough surfaces, the old approximation was overly conservative.

Section 2: Inspection set-ups and physical properties

Inspection qualification is a highly developed formal activity in the UK, implemented in accordance with the European Network for Inspection and Qualification (ENIQ) methodology [1], and uses a variety of resources for the technical justification part of the qualification: capability evaluation exercises, site experience, applicable and validated theoretical models, physical reasoning and test-piece experimentation.

The model presented here is designed to be adopted within inspection qualification as an applicable theoretical model, having been validated by numerical and experimental methods for appropriate ranges of validity [4-7]. The model is versatile, being applicable for a range of inspection set-ups, such as pulse-echo (P-E) and pitch-catch, as well as including capability for the inclusion of tilt and skew angles. Here, we concentrate on determining expected amplitudes for specular and back-scattered directions for a range of P-E set-ups that include tilted defects, as illustrated in Figure 3.

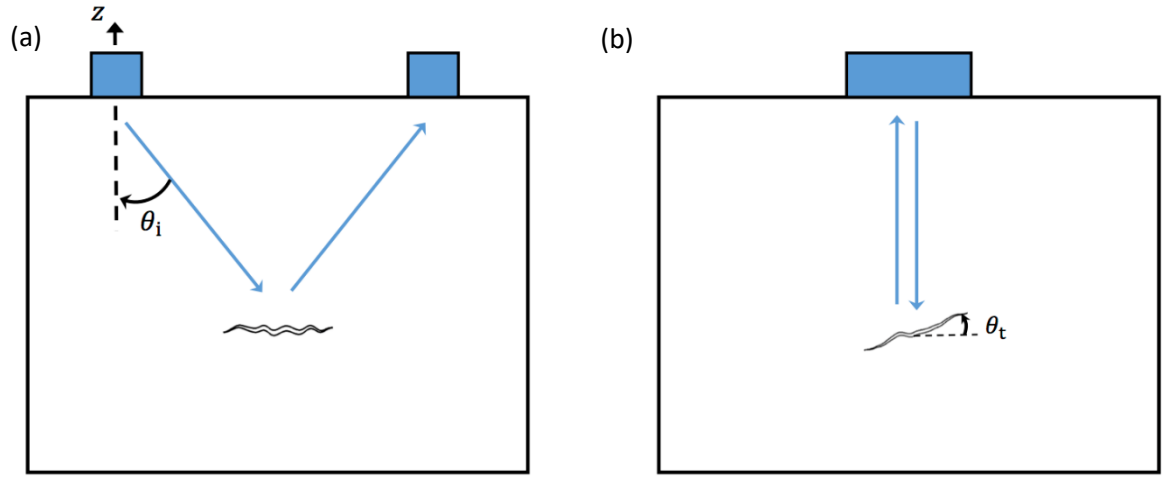

Figure 3: Schematic diagrams of inspection set-ups simulated by model. **(a)** Pitch-catch with θ_{i} representing the beam angle. **(b)** Pulse-echo with θ_{t} representing the tilt angle of the defect.

As explained in detail in the publications [4-7], the new statistical elastodynamic scattering model applies a stationary phase method to the Kirchhoff approximation (KA) displacement term to derive expected diffuse intensity formulae for rough surfaces for *any* scattering direction. This universality improves on the estimate for diffuse intensity given in preceding work [3], where the diffuse term was calculated as an average over all scattering angles. For the case of very rough surfaces, for which

any specular preference vanishes, the original assumptions [3] produced good qualitative trends, but overly conservative quantitative predictions compared with the new approach, which shows a huge improvement for medium-to-high roughness (e.g. for $\sigma > 0.1\lambda_p$ in Figure 1).

2.1 Quantification of Roughness

The roughness of a surface is typically characterized by two statistical parameters [15], the standard deviation σ, or root mean square (RMS) value, of height relative to a reference surface, and the lateral correlation length λ_0, which determines the statistical independence of a rough surface's peaks and troughs. The RMS height may be defined formally as:

$$\sigma = \sqrt{\langle h^2 \rangle}, \quad \langle h \rangle = \int_{-\infty}^{\infty} h\, p(h)\, dh = 0, \tag{3}$$

where $p(h)$ is a probability density function and $\langle \quad \rangle$ denotes spatial averaging over the surface. A correlation function describes the extent to which information about the height at one point on a surface determines, on average, the height at another point [16]. In two-dimensional (2D) space, a normalized correlation function $C(R)$ is defined as:

$$C(R) = \frac{\langle h(x)h(x+R) \rangle}{\sigma^2}, \tag{4}$$

where x and h are defined as in Figure 4, and R is the distance between any two points on the surface. Note that $C(0) = 1$ and usually $C(\infty) = 0$ so that as R increases, $C(R)$ falls. The correlation length λ_0 is the distance over which $C(R)$ falls to $1/e$.

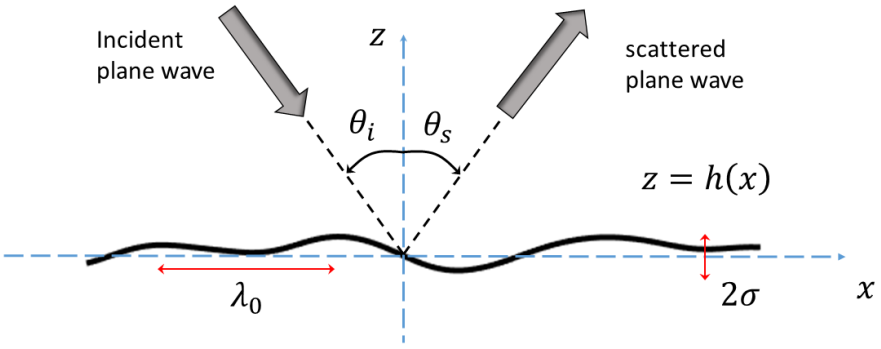

Figure 4: A schematic rough surface illustrating the statistical roughness parameters σ and λ_0 in 2D-space. Note that the height above the mean surface $z = 0$ is a function of the lateral variable x, and that the incident and scattering angles of a plane wave are θ_i, θ_s.

Note that we follow previous literature [6,7] in using two-dimensional space in this article to investigate a wider range of parameters owing to the increased computational efficiency; the equivalent definitions and expressions are provided in 3-dimensional space in [4,5]. In addition, the mechanisms that determine the limits of validity for KA are equivalent in 2D and 3D [17] and quasi-2D cracks are common in practice, for example in welds [18].

We follow the literature in choosing Gaussian distributions for both height and correlation functions:

$$p(h) = \frac{1}{\sigma\sqrt{2\pi}} \exp\left(-\frac{h^2}{2\sigma^2}\right), \quad C(R) = \exp\left(-\frac{R^2}{\lambda_0^2}\right). \tag{5}$$

As noted by Ogilvy [3], both statistical and experimental studies identified classes of rough surfaces for which distributions are close to Gaussian. Fatigue and corrosion measurements [18-20] have also supported this conjecture and recently, Choi et al. [21] identified specific regimes for which Gaussian distributions approximate real rough surfaces well.

2.2 Coherent and diffuse fields

The total intensity is the sum of coherent and diffuse parts:

$$I^{\mathrm{t}} = I^{\mathrm{c}} + I^{\mathrm{d}}. \tag{6}$$

An important expression, widely used in industry, to estimate the coherent contribution for a rough surface defined by σ is [3,22]:

$$I^{\mathrm{c}} = I^{\mathrm{fs}} \exp\left(-g_{\alpha\beta}\right), \qquad g_{\alpha\beta} = \left(k_\alpha \cos\theta_{\mathrm{i}} + k_\beta \sin\theta_{\mathrm{s}}\right)^2 \sigma^2, \tag{7}$$

where α and β indicate, respectively, the incident and scattered wave-types. As usual, k_α, k_β are wavenumbers. The intensities I^{c} and I^{fs} represent, respectively, a rough surface's coherent part and the analogous smooth surface (i.e. same angle of incidence and length) scattering intensity. The expression for I^{c} in (7) provides accurate predictions but our breakthrough is in deriving a theoretical expression for I^{d}. It is well known that as roughness increases, the diffuse field I^{d} begins to dominate [14,15]. The new formula for the expected diffuse intensity, and hence to evaluate the total intensity via (6), is

$$I^{\mathrm{d}}_{\alpha\beta}(D) = \frac{k_\beta F^2_{\alpha\beta} L \lambda_0 \sqrt{\pi} e^{-g_{\alpha\beta}}}{2\pi D} \sum_{m=1}^{M} \frac{g^m_{\alpha\beta}}{m!\sqrt{m}} \exp\left[-\frac{k_\beta^2 A^2_{\alpha\beta} {\lambda_0}^2}{4m}\right], \tag{8}$$

where $F_{\alpha\beta}$ is termed the elastodynamic factor which, along with the phase term $A_{\alpha\beta}$, depends on incident and scattering angles and material parameters. The full expressions and derivations for these roughness-independent terms are provided in [4] and [7]. The sum in (8) is such that M is a relatively small integer ($M = 20$ is more than sufficient for the range of validity where the model applies). Although the formula (8) is more complicated than the coherent formula (7), its computation also takes less than 1 second on a standard computer. The user requires the following inputs to obtain the diffuse field:

- Length of defect, L
- Angle of incidence, θ_{i}
- Scattering angle, θ_{s}
- RMS height, σ (embedded within $g_{\alpha\beta}$)
- Correlation length, λ_0
- Material parameters
- Wave-type (shear or compression)
- Transmit-receive locations (*D* is the distance from defect to receiver)

Comparing this list with the inputs required for (7), there is only one different parameter: the correlation length. The complexity of (8) is embedded within $F_{\alpha\beta}$, which uses a Stationary Phase Approximation (to remove surface-specific dependence) of the Reflection derived using KA (SPARK);

the result is a theoretical ensemble average formula. The procedure is explained in detail for compression waves in [4], and for shear waves, in [7]. We limit ourselves here to identify ranges of physical parameter and roughness values for which the method may be applied and has been validated. We also note that formula (8) is specific to a Gaussian correlation function (5); similar expressions may be derived for alternative correlation function definitions.

2.3 Ranges of validity for 2D SPARK

Defects ranging from 4mm to 8mm have been extensively investigated for the 2D case for incident compression [4,5] and shear [6,7] waves, for frequencies ranging from 2MHz to 10MHz. Our validations have concentrated on two materials, aluminium (E=70GPa, ρ=2700kg/m^3, ν=0.33; c_p=6200m/s, c_s=3120m/s) and stainless steel (E=210GPa, ρ=7800kg/m^3, ν=0.29; c_p=5940m/s, c_s=3230m/s). In most cases, the crack length $L \geq 5\lambda_{\mathrm{inc}}$, ensuring that tip diffraction signals (which are not taken into account by KA) are negligible and do not affect the validation of the new model's reflection predictions. Experiments using a CNC-milled (computer numerical control) aluminium block were performed for compression [4] and shear [7] incidence for corrugated rough surfaces, but most validations were carried out using the high-fidelity finite element software Pogo [23].

The range of validity for the SPARK model is intrinsically linked to the range of validity for KA with which the scattering of an individual surface may be modelled. The recent results provided by [4,5] for compression waves, and [6,7] for shear waves are used to complete Table 1 that summarizes the validation work carried out for 2D cases. The SPARK model is also applicable to the 3D case, as explained in [4] but 2D examples are featured here to cover a larger range of parameter values.

Wave-type	Crack length (mm)	Incident angles (°)	Scattering angles (°)	λ_0 (λ_{inc})	σ (λ_{inc})	λ_0 (mm)	σ (mm)	$\frac{\lambda_0}{\sigma}$
Compression	≥ 6	$-45 \leq \theta \leq 45$	$-80 \leq \theta \leq 80$	1/4 to 1	1/64 to 1/2	0.15 to 2.4	0.01 to 1.2	>1
Shear	≥ 4	$-20 \leq \theta \leq 20$	$-60 \leq \theta \leq 60$	1/4 to 2	1/64 to 1/2	0.15 to 2.5	0.005 to 0.64	>4

Table 1: Summary of defect lengths, incident and scattering angles, roughness parameters validated for aluminium and stainless steel.

The most important column in Table 1 is highlighted; the thresholds of validity for KA and therefore equation (8), using the ratio of roughness parameters, differ for compression and shear wave incidence [6,7]. Provided that the inequalities $\lambda_0 / \sigma > 1$ for compression incidence and $\lambda_0 / \sigma > 4$ for shear waves are satisfied, KA and the SPARK ensemble average formulae are valid for the cases we have investigated. Other results in the literature such as the longitudinal cases [14,18], investigated using scattering matrix methods, are consistent with Table 1.

Section 3: Monte Carlo studies of Gaussian rough surfaces

The validation procedure for the 2D SPARK model involves generating datasets of rough surfaces characterized by a specified pair (λ_0, σ) to run Monte Carlo analysis. Typically, 200-400 realisations were generated for FE simulations, using the standard weighted moving average method [15]. The

details of the FE methods are provided in [4-7]. Key parameter settings are summarized in Table 2, with the specified values corresponding to the examples of Figures 5-8 shown here.

Material	Distance *D* (mm)	Incident angle (°)	Defect length (mm)	Centre Frequency (MHz)	Wave-type	Mesh size (mm)	Number of surfaces
Stainless steel	50	0	8	5	compression	0.025	200

Table 2: Summary of the parameters required for FE Monte Carlo analysis. The specified values were used for the illustrative examples of Figures 5-8.

Following the literature [5,6], the KA is deemed valid provided that the mean amplitude/intensity in the backscattered direction, obtained from the FE and KA methods, differs by ≤ 1dB. An individual FE simulation takes around 3 minutes and for low roughness cases, 200 realisations is more than sufficient for convergence when validating the FE models with the KA predictions. Previous reports [14] used 50 realisations to demonstrate convergence for roughness within the range of validity for KA. For roughness values close to the upper limit of KA validity, 400 FE surfaces were analysed here; this is consistent with previous literature [2] in which explanations for the necessity of increasing the number of simulations is provided.

An example is illustrated in Figures 5-7 for $\lambda_0 = \lambda_p/2 = 0.59$mm, $\sigma = \lambda_p/8 = 0.15$mm, with $\lambda_0 \,/\, \sigma = 4$, a case for which KA and SPARK are valid (see Table 1).

(a) (b)

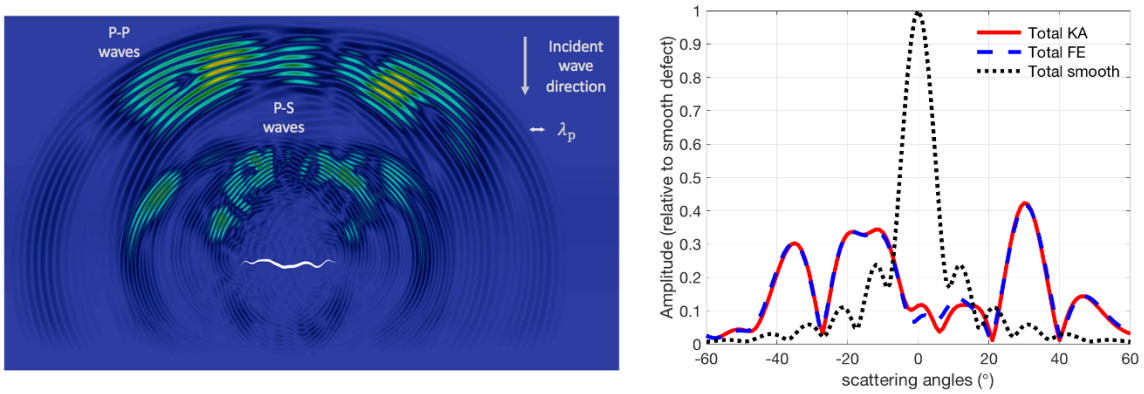

Figure 5: (a) FE scattered signal for an individual realisation with $\lambda_0 = \lambda_p/2 = 0.59$mm, $\sigma = \lambda_p/8 = 0.15$mm for normally incident 5MHz compression waves. **(b)** Normalised reflection amplitude (relative to a smooth 8mm defect) vs. scattering angle for both KA and FE models for the defect in (a).

The scattering from one of the 200 surfaces is depicted in Figure 5(a) with the scattered field generated using Pogo [23]. The direction of the incident wave is shown by the arrow in the top right corner. The reflected P-P and P-S waves are also labelled and the colour gradients represent the displacement amplitude at a moment in time after they have reflected from the defect. Receivers were located in the far field and the associated reflection amplitude spectrum for this specific case is illustrated in Figure 5(b), along with the smooth defect's signal used to normalize amplitudes to a

unit scale. There is very good agreement between the FE and KA models. The ensemble average of the backscattered amplitude over the full dataset of 200 surfaces, calculated using equation (1), is shown in Figure 6. Again, there is very little difference between the two approaches, with the mean amplitude being 40% of the smooth defect's signal.

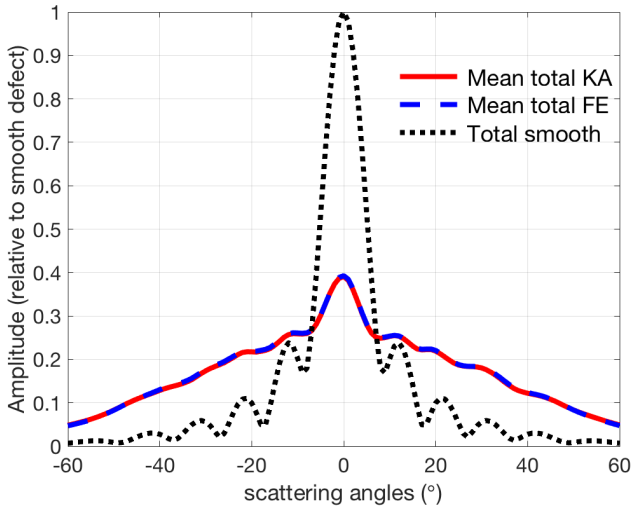

Figure 6: Mean total amplitude (relative to smooth 8mm defect) versus scattering angle for KA and FE models for 200 surfaces with $\lambda_0 = \lambda_p/2 = 0.59$mm, $\sigma = \lambda_p/8 = 0.15$mm insonified by normally incident 5MHz compression waves.

In addition, it appears that signal levels from rough defects at normal incidence are appreciably lower than for smooth defects, but reach higher levels in non-specular directions. This observation is consistent with experimental measurements made by Toft [24] for a set of larger defects (25mm).

Section 3.1: Conversion of expected intensity to expected amplitude

In order to compare Monte Carlo results with the SPARK prediction, the intensity values are required. Comparing equations (1) and (2), the ensemble average for amplitude is the mean of the moduli of the individual displacements, whilst the analogous intensity value is the mean of the squares. This latter value is compared with the predicted value obtained from the sum of equations (7) and (8) to give equation (6) to assess the validity of the SPARK model.

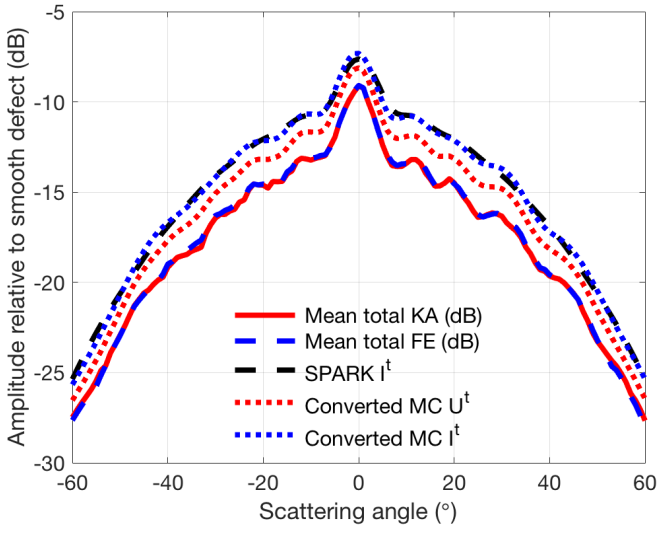

Figure 7: Mean total intensity and amplitude (relative to smooth 8mm defect) on dB scale versus scattering angle for KA and FE models for 200 surfaces with $\lambda_0 = \lambda_p/2 = 0.59\text{mm}$, $\sigma = \lambda_p/8 = 0.15\text{mm}$ insonified by normally incident 5MHz compression waves.

However, in practice, amplitude measurements are taken on a dB scale. Figure 7 illustrates the conversion of the results displayed in Figure 6 to the dB scale, plus the analogous intensity curves. The standard conversion formulae are:

$$I^{\mathrm{t}}(\mathrm{dB}) = 10\log_{10}(I^{\mathrm{t}}), \quad U^{\mathrm{t}}(\mathrm{dB}) = 20\log_{10}(U^{\mathrm{t}}) = 10\log_{10}(U^{\mathrm{t}})^2. \tag{9}$$

Therefore, the theoretical prediction of I^{t} obtained from (6)-(8) is converted to dB using equation (9), producing the black dashed line in Figure 7. If the same formulae are applied to the FE mean intensity and the FE mean amplitude (shown in Figure 6), we obtain the dotted blue and red curves, respectively. Note the very close match between the intensity curve and the SPARK prediction. The amplitude curve, though, shows deviation from the other two, emphasizing that the square of the mean, $(U^{\mathrm{t}})^2$, is not equal to the mean of the squares I^{t} and that there is not a straightforward conversion between the ensemble averages for amplitude and intensity, i.e.

$$\left(\frac{1}{N}\sum_{n=1}^{N}|u_n^{\mathrm{sc}}(\theta_{\mathrm{sc}})|\right)^2 \neq \frac{1}{N}\sum_{n=1}^{N}|u_n^{\mathrm{sc}}(\theta_{\mathrm{sc}})|^2 . \tag{10}$$

However, to derive meaningful confidence bands for the predicted intensity/amplitude values on a dB scale, the mean and standard deviation are calculated directly on the log scale, by first converting the original individual normalized amplitude values (i.e. between 0 and 1) with $20\log_{10}(|u_n^{\mathrm{sc}}(\theta_{\mathrm{sc}})|)$. This produces identical values for the amplitude and intensity for each individual realization on the log scale after application of the conversion formulae given in (9). The solid red and dashed blue curves in Figure 7 show this, as well as a notable difference between these curves and the SPARK prediction. Figure 8 illustrates how to convert the theoretical prediction for intensity to a prediction for practical amplitude measurements.

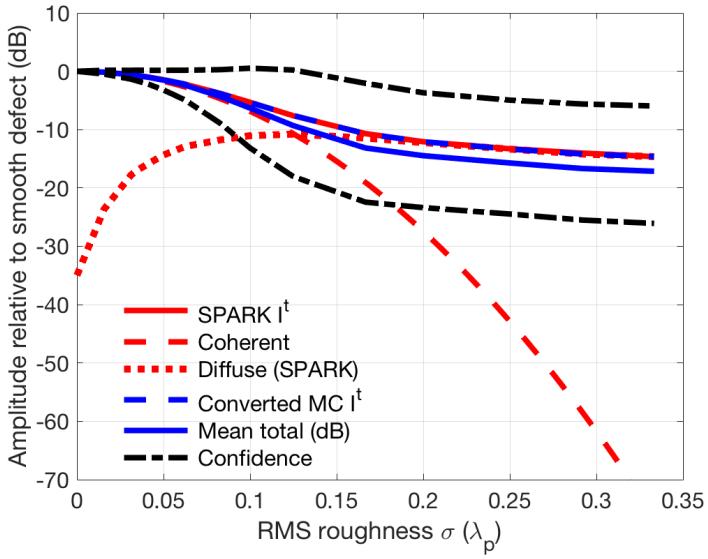

Figure 8: *Expected reflection amplitude (relative to a smooth defect of the same size, 8mm) vs RMS roughness (measured in incident wavelengths) for normally incident compression waves in a Pulse-Echo set-up with centre frequency 5MHz. The solid red line is the predicted P-P intensity using the SPARK model, with the dashed and dotted red lines representing the coherent and diffuse parts. The*

solid blue line shows the MC amplitude mean calculated directly in dB (the converted mean is dashed blue), with the confidence bands (± 2 standard deviations) denoted by black dot-dashed curves.

Once the coherent part of the scattered field is no longer dominant, the curves for theoretical intensity and amplitude deviate but with a maximum difference of 2.5dB for all frequencies and roughness values considered. Therefore, a simple and safe conversion for $\sigma > 0.1\lambda_{\mathrm{inc}}$ would be:

$$U_{\mathrm{dB}}^{\mathrm{t}} = 10\log_{10}(I^{\mathrm{t}}) - 2.5, \tag{11}$$

where I^{t} is obtained from equations (6-8) and would be obtained rapidly for a given set of parameter values. Note that the confidence bands (based on MC KA data for 4000 surfaces for each roughness), cover ± 2 standard deviations. The lower confidence band in Figure 8 has a minimum value -26dB, considerably higher than the conservative estimates for the actual scattering amplitude from the model of [3].

Section 4: Validation using realistic thermally fatigued surfaces

The new intensity formulae provide quick and accurate predictions for the ultrasonic response scattered by a rough defect generated using Gaussian height and correlation distributions. The model is also effective when applied to realistic rough surfaces. Twenty thermally fatigued stainless steel 304L samples (provided and scanned courtesy of Rolls-Royce) were tested with the SPARK model. An example is shown in Figure 9, with a photograph and the reproduced contour plot of the measured dataset (scanned using an Alicona optical microscope). The samples were obtained via specimen separation or 50% load drop, with the resulting datasets processed and statistically characterised.

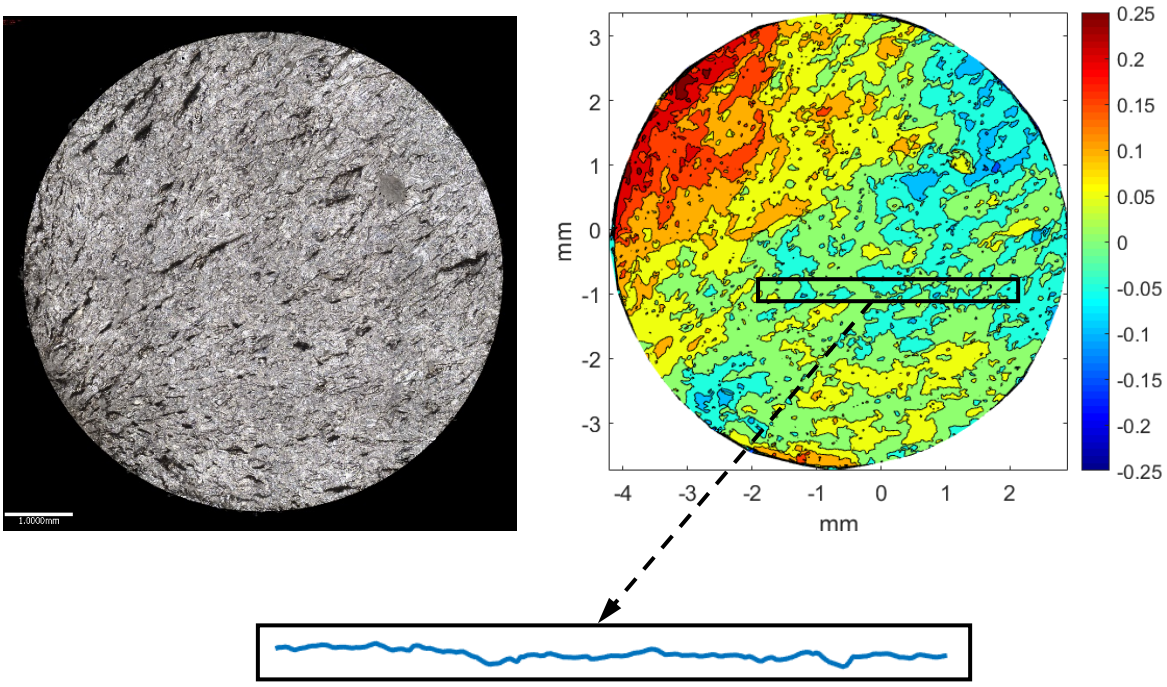

Figure 9: 304L stainless steel thermally fatigued sample (courtesy of Rolls-Royce) with reproduced contour plot (in mm) and an extracted 4mm rough defect with $\lambda_0 = 0.25$mm, $\sigma = 0.03$mm.

The values obtained for (λ_0, σ) for fatigue in steel are consistent with previous literature [2,21]. Values from 0.01 up to 0.5mm were reported for RMS height σ in A533B samples by [2], and [21] reported an average correlation length of 0.563mm in A533B.

More than 800 1D 304L samples of length 4mm (as magnified in Figure 9) were evaluated here, with ranges of:

$$0.1\text{mm} \leq \lambda_0 \leq 1.8\text{mm}, \;\; 0.02\text{mm} \leq \sigma \leq 0.1\text{mm}.$$

However, more than 60% of the samples were such that $0.1\text{mm} \leq \lambda_0 \leq 0.6\text{mm}$, with accompanying σ values such that the resultant ratios $\lambda_0 \,/\, \sigma$ ranged from around 5 to 20. In Figures 10 and 11, we present results for 140 surfaces with $\lambda_0 = 0.25\text{mm}$ and σ varying from 0.02 to 0.045mm. Numerical validations for these realistic rough surfaces were performed using shear wave incidence with the parameter values given in Table 3.

Material	Distance D (mm)	Incident angle (°)	Defect length (mm)	Centre Frequency (MHz)	Wave-type	Mesh size (mm)	λ_{inc} (mm)
Stainless steel 304L	40	-5	4	5	shear	0.025	0.646

Table 3: Parameters used in FE and KA simulations for validation of SPARK method using a set of 140 thermally fatigued samples in 304L.

Figure 10(a) shows the reflection amplitude spectrum for a single 4mm defect on the dB scale. The total amplitude for both KA (solid red) and FE (dashed blue) are shown for 5MHz shear waves incident at $-5°$, along with the normalization result for a smooth defect (normally incident 5MHz shear). There is good agreement between the KA and FE results near the specular angle ($-5°$) but the agreement deteriorates at exterior scattering angles, as a result of tip signals that KA does not account for [15].

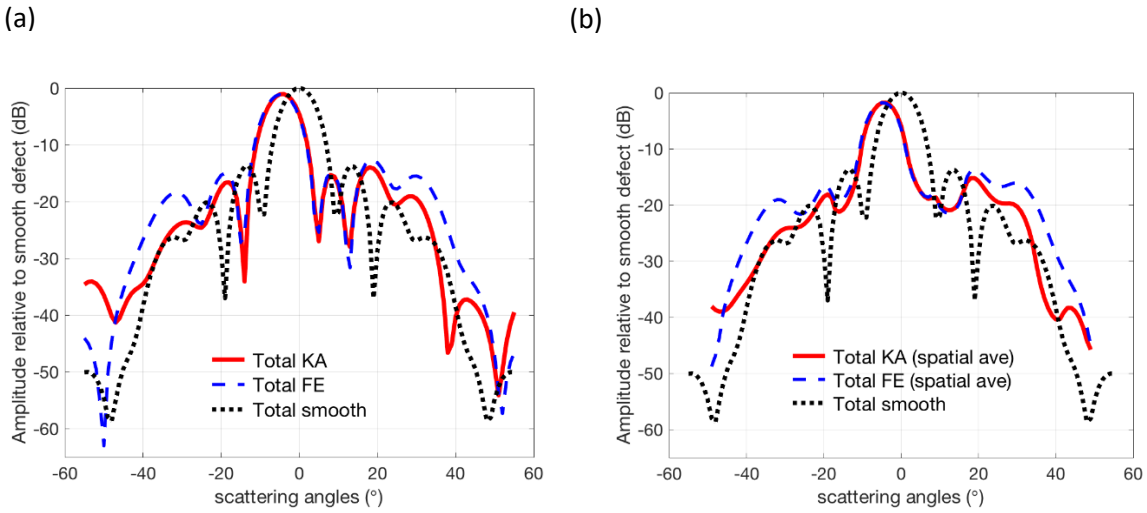

Figure 10: (a) Scattering spectrum for shear-shear mode for thermally fatigued 4mm defect (5MHz) for angle of incidence $\theta_{\text{i}} = -5°$. **(b)** Spatially averaged amplitude spectrum of part **(a)** with each average calculated over $\pm 3°$ for each θ_{s} plotted at $1°$ intervals.

Another notable feature of Figure 10(a) is the collection of sharp dips which arise due to interference. In practice, in a scanned inspection, multiple angles are used for detection within the spread of a beam and this will mitigate sharp dips in intensity. Therefore, the worst case value in practice is highly likely

to be better than that shown in Figure 10(a). In order to reveal more realistic predictions for a single realisation, our method includes the capability for obtaining a spatial average in the time (FE) and frequency (KA) domains by computing the mean over a specified range of scattered angle increments for any scattering direction. Figure 10(b) illustrates the case for the spatial average calculated over values $\pm 3°$ either side of the plotted scattering angle. The dips in amplitude at around -15°, 5°, 12°, 35° etc. in Figure 10(a) have all been *smoothed* in Figure 10(b), which presents a more realistic set of results for a field engineer conducting a component inspection.

Figure 11 illustrates a MC validation of the SPARK predictions based on 140 surfaces characterized by $\lambda_0 = 0.25\text{mm}$, $0.019\text{mm} \leq \sigma \leq 0.045\text{mm}$, and ratio $5.5 \leq \lambda_0 / \sigma \leq 13.5$, which satisfy the condition for KA and SPARK validity for shear waves in Table 1. As expected, the agreement is extremely good between the SPARK prediction for the total intensity I^{t} (solid black curve) and the MC result for the mean intensity converted to dB using equation (9). For completeness, we include the spatially averaged mean amplitudes for KA (solid red) and FE (dashed blue), which are calculated by finding the means after the individual amplitudes have been converted to dB. Since $\sigma < 0.1\lambda_{\text{inc}}$, note that the specular prediction for intensity matches that of the MC amplitudes on the dB scale so the 2.5dB correction in equation (11) would not be applied in this case.

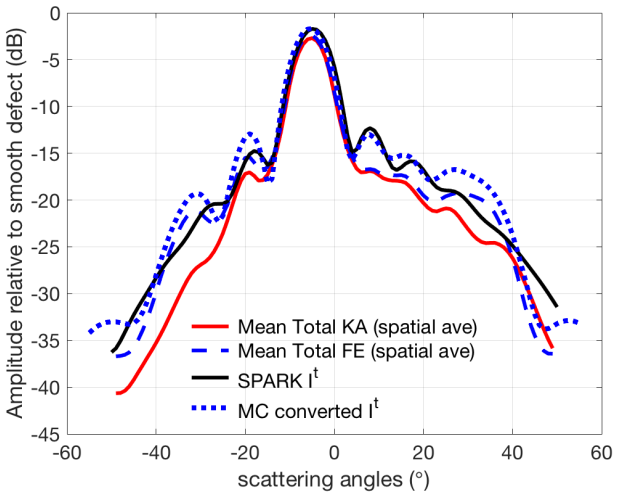

Figure 11: SPARK I^{t}, mean total intensity (MC converted into dB) and mean total amplitudes (spatially averaged) for 140 thermal fatigue 304L samples; 5MHz shear waves incident at $\theta_{\text{i}} = -5°$.

Section 5: Effect of defect tilt on backscattered signal from rough defects

Modelling is most valuable when it reveals important and statistically significant effects for application in practice. The SPARK scattering intensity predictions are particularly useful since a variety of parameters and set-ups can be investigated efficiently. We present a case study for the effect of tilt on the backscattered signal for rough defects. Referring to Figure 3(b), a preliminary study was conducted for frequency, tilt angle and roughness settings. As tilt angle θ_{t} increases from 0 to $15°$, once a certain roughness threshold has been reached, SPARK predicts that the backscattered signal converges regardless of θ_{t} value.

An example is shown in Figure 12 for two frequencies (2.5MHz and 5MHz) for compression waves. The roughness values (in mm) are identical for each frequency and the pairs of curves for each of $5°, 10°, 15°$ (denoted by blue, red and black curves respectively) were obtained using SPARK. All curves

are normalized with respect to the normally incident backscattered reflection for a smooth defect (with 0 tilt) of the same length, 8mm. The 2.5MHz predictions are indicated by the dashed curves, which start to converge at $\sigma = 0.4$mm, the upper end of KA roughness validity for 5MHz. The convergence for the 5MHz cases is clear and the 2.5MHz predictions indicate the same trend. Note that a broader amplitude peak for the lower frequency produces a significantly higher backscattered signal for $\theta_t = 5°$. All other curves feature the characteristic increase to a peak backscattered amplitude before flattening.

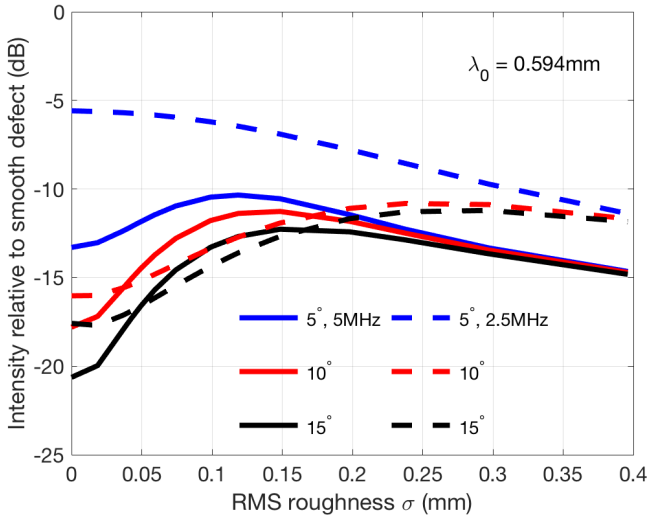

Figure 12: SPARK predictions of backscattered total intensity for tilted rough defects insonified by 2.5MHz and 5MHz compression waves. Fixed $\lambda_0 = 0.594$mm, with σ plotted on the horizontal axis. Tilt angles are $5°, 10°, 15°$ (blue, red, black curves) with 2.5MHz denoted by dashed lines. Intensity is normalized with respect to the 0 tilt case for a smooth 8mm defect.

The predicted convergence of backscattered amplitudes appears independent of tilt angle and arises for typical NDE centre frequencies, 2.5, 5 and 10MHz. Validation analysis was conducted using MC methods for both KA (4000 surfaces) and FE (400 surfaces). The parameter settings for these investigations are summarized in Table 4.

Wave type	Frequency (MHz)	Tilt angle (°)	Range of λ_0 (mm)	Range of σ (mm)	No. of surfaces KA	No. of surfaces FE	Material
Compression	2.5,5,10	0,5,10,15	0.3-0.6	0.01-0.4	4000	400	Stainless steel
Shear	2.5,5,10	0,5,10,15	0.32-0.65	0.005-0.21	4000	400	Stainless steel

Table 4: Parameters used for MC validation of tilt angle convergence of backscattered signals in Pulse-Echo inspection set-ups.

For critical values of σ, i.e. those values for which SPARK predicted convergence regardless of θ_t, additional FE simulations were run over 400 realisations, since the error between KA and FE results increases for higher values of roughness and tilt angle.

Examples for both compression and shear incidence are illustrated in Figure 13. The spatially averaged amplitudes (explained in Section 4) are plotted versus σ for fixed correlation length for 10MHz compression waves in Figure 13(a), and for 5MHz shear waves in Figure 13(b). Once again, confidence bands of ± 2 standard deviations are denoted by dashed black curves (upper for $5°$ and lower for $15°$) and the results for 0 tilt (dashed red) are included for reference. The FE results for $\lambda_{\text{inc}}/_5, \lambda_{\text{inc}}/_4, \lambda_{\text{inc}}/_3$ are plotted with markers, $\mathrm{O}, +, \times$ for $5°, 10°, 15°$ respectively.

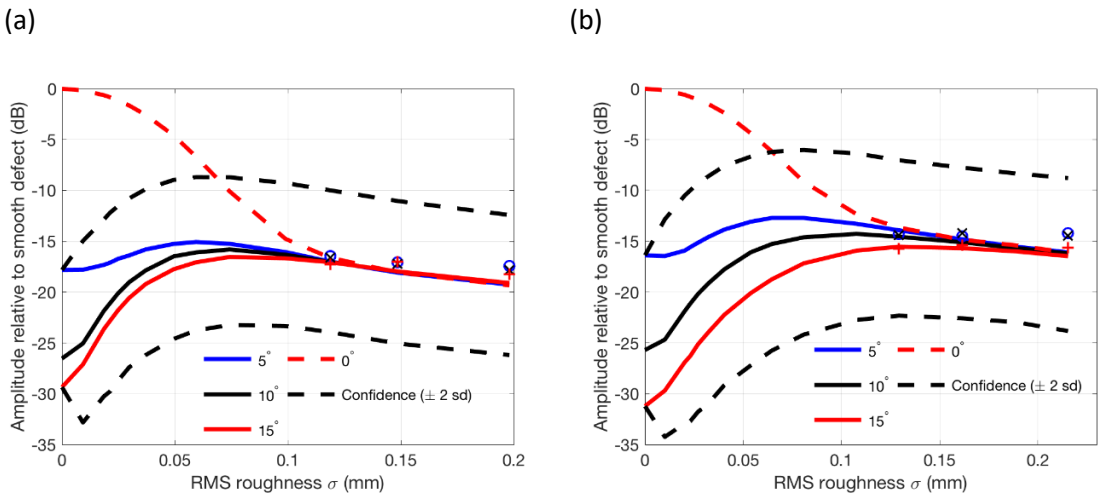

Figure 13: MC (4000 surfaces) KA backscattered amplitude (relative to smooth 8mm defect) scattered by tilted defects ($5°, 10°, 15°$) with 0 tilt shown by dashed red curve. Confidence bands of 2 standard deviations are also included. **(a)** Incident 10MHz compression waves for $\lambda_0 = 0.297$mm. **(b)** Incident 5MHz shear waves for $\lambda_0 = 0.646$mm. FE results for 400 realisations are also shown for each tilt angle (using markers) for $\sigma = \lambda_{\text{inc}}/_5, \lambda_{\text{inc}}/_4, \lambda_{\text{inc}}/_3$.

The results of Figure 13 indicate that the convergence is observed for both the KA and FE numerical experiments, for multiple frequencies and for both compression and shear waves. These observations are consistent with experimental studies on the effect of misorientation carried out by Toft [24] for 25mm brittle fracture faces. For shear and compression wave incidence, and RMS values of up to one quarter of a wavelength, measurements were made showing that moderate detectability was maintained in the backscattered direction for misorientations up to $50°$ [23].

Section 6: Concluding remarks and outlook

We have presented a new analytical approach (SPARK) based on a stationary phase treatment of the reflected part of the scattered field, derived using Kirchhoff Approximation, for a rough planar defect. The statistical model predicts the expected scattering amplitude in under 1 second (on a standard computer), and shows significant improvement over models originally derived in the 1980s [3]. All the mathematical details are available in the publications [4-8] and here we have summarized relevant ranges of applicability and validated cases. The examples presented include realistic thermally fatigued samples in 304L stainless steel, and cover compression and shear wave incidence, including all mode conversions. The dimensions of the featured defects are such that the effect of tips has minimal effect, ensuring that the validation of SPARK using numerical and experimental methods was optimized.

The model is very versatile and can be deployed for a variety of applications and defect descriptions of desired industrial interest beyond the case studies presented in this article. The SPARK model for reflected signals from isotropic media may be coded by interested readers using the equations in this article and [4-8]; it is intended that a user-friendly code will be developed by the authors to be suitable for application in technical justification within inspection qualification.

One of the great assets of the model is its speed which enables large scale, statistically significant studies to be performed. A case study was included here showing that for defects representative of those that can occur in plant, the tilt angle is likely to have little effect on expected reflection amplitude for medium-to-high roughness cases. This is consistent with experimental observations recorded by [24]. Tilt angles up to $\pm 15°$ display this property for Pulse-Echo shear and compression incidence for centre frequencies ranging from 2.5MHz to 10MHz. Therefore rough defects can be detected at a predictable, but moderate, signal amplitude regardless of tilt. We have also shown that for settings where defects are expected to be very rough, reliable predictions, with known confidence bounds, may be made for the expected reflection amplitudes without precise knowledge of the surface profile or RMS height.

Acknowledgements

The authors gratefully acknowledge the support of the EPSRC through the Grant reference number EP/P01951X/1 and our industrial partners: Rolls-Royce, EDF Energy, Jacobs Engineering, National Nuclear Laboratory and BAE Systems. PH acknowledges the support of the EPSRC through the Fellowship reference number EP/M020207/1. The authors also express their gratitude to Professor Will Daniels and Dr Tim Skinner for discussions and their very helpful comments and suggestions.

References

[1] C Curtis, A Walker and I Atkinson, `Inspection Qualification and NDE Reliability', *Proceedings of 58th Annual Conference of the British Institute of Non-Destructive Testing-NDT*, 2019.

[2] J Pettit, A Walker and M J S Lowe, `Improved Detection of Rough Defects for Ultrasonic Nondestructive Evaluation Inspections Based on Finite Element Modeling of Elastic Wave Scattering', *IEEE Trans UFFC*, Vol 62, No 10, pp 1797-1808, 2015.

[3] J A Ogilvy, `Theoretical comparison of ultrasonic signal amplitudes from smooth and rough defects'. *NDT International*, Vol 19, No 6, pp 371-385, 1986.

[4] F Shi, M J S Lowe, X Xi and R V Craster, `Diffuse scattered field of elastic waves from randomly rough surfaces using an analytical Kirchhoff theory', *J. Mech. Phys. Solids,* Vol 92, pp 260–277, 2016.

[5] F Shi, W Choi, M J S Lowe, E A Skelton and R V Craster, `The validity of Kirchhoff theory for scattering of elastic waves from rough surfaces', *Proc. Roy. Soc. A*, Vol 471**,** 20140977, 2015.

[6] S G Haslinger, M J S Lowe, P Huthwaite, R V Craster and F Shi, `Appraising Kirchhoff approximation theory for the scattering of elastic shear waves by randomly rough defects', *Journal of Sound and Vibration,* Vol 460, 114872, 2019.

[7] S G Haslinger, M J S Lowe, P Huthwaite, R V Craster and F Shi, `Elastic shear wave scattering by randomly rough surfaces', *J. Mech. Phys. Solids*, Vol 137, 103852, 2020.

[8] F Shi, M J S. Lowe and R V Craster, `Diffusely scattered and transmitted elastic waves by random rough solid-solid interfaces using an elastodynamic Kirchhoff approximation', *Phys. Rev. B,* Vol 95, No 21, 214305, 2017.

[9] F G Bass and I M Fuks, *Wave Scattering from Statistically Rough Surfaces,* Oxford, UK: Pergamon Press, 1979.

[10] E I Thorsos, `The validity of the Kirchhoff approximation for rough surface scattering using a Gaussian roughness spectrum', JASA, Vol 83, No 1, pp 78-92, 1988.

[11] J A Ogilvy, `Model for the ultrasonic inspection of rough defects', *Ultrasonics*, Vol 27**,** No 2, pp 69–79, 1989.

[12] J A Ogilvy and I D Culverwell, `Elastic model for simulating ultrasonic inspection of smooth and rough defects', Ultrasonics, Vol 29, pp 490-496, 1991.

[13] S F Burch, N Collett, R K Chapman and M W Toft, `Experimental validation of the TRANGLE and related NDT codes for modelling the ultrasonic inspection of rough cracks', *Insight*, Vol 46, No 2, pp 74–76, 2004.

[14] J Zhang, B W Drinkwater and P D Wilcox, `Longitudinal Wave Scattering From Rough Crack-Like Defects', *IEEE Transactions on Ultrasonics, Ferroelectrics, and Frequency Control*, Vol 58, No 10, pp 2171-2180, 2011.

[15] J A Ogilvy, Theory of Wave Scattering from Random Rough Surfaces, CRC Press, 1991.

[16] J A Ogilvy and J R Foster, `Rough surfaces: Gaussian or exponential statistics?', Journal of Physics D: Applied Physics, Vol 22, pp 1243-1251, 1989.

[17] R A Roberts, `The effect of crack morphology on ultrasonic response', *AIP Conference Proceedings*, Vol 1430, No 1, American Institute of Physics, 2012.

[18] J Zhang, B W Drinkwater and P D Wilcox, `Effect of roughness on imaging and sizing rough crack-like defects using ultrasonic arrays', *IEEE Transactions on Ultrasonics, Ferroelectrics, and Frequency Control*, Vol 59, No 5, pp 939-948, 2012.

[19] P Nagy and L Adler, `Surface roughness induced attenuation of reflected and transmitted ultrasonic waves', JASA, Vol 82, No 1, pp 193-197, 1987.

[20] M Stone, `Statistical analysis methods for corrosion mapping inspection data', *Insight,* Vol 53, No 2, pp 76-81, 2011.

[21] W Choi, F Shi, M J S. Lowe, E A Skelton, R V Craster and W L Daniels, `Rough surface reconstruction of real surfaces for numerical simulations of ultrasonic wave scattering', *NDT & E International*, Vol 98, pp 27-36, 2018.

[22] M de Billy, F C Tenoudji, G Quentin, K Lewis and L Adler, `Ultrasonic evaluation of geometrical and surface parameters of rough defects in solids', *J. NonD. Eval.*, Vol 1, No 4, pp 249-261, 1980.

[23] P Huthwaite, `Accelerated finite element elastodynamic simulations using the GPU', *Journal of Computational Physics,* Vol 257, pp 687-707, 2014.

[24] M Toft, `Experimental studies of ultrasonic reflection from various types of misoriented defect', *Proceedings of 21st Annual Conference of the British Institute of Non-Destructive Testing-NDT,* 1986.